energies

MDPI

Article

Study on Surface Condensate Water Removal and Heat Transfer Performance of a Minichannel Heat Exchanger

Xiuli Liu [1], Hua Chen [1,*], Xiaolin Wang [2] and Gholamreza Kefayati [2,*]

[1] Laboratory of Refrigeration Technology of Tianjin, Tianjin University of Commerce, Tianjin300134, China; liuxiuli@stu.tjcu.edn.cn

[2] School of Engineering, University of Tasmania, Hobart, TAS 7001, Australia; Xiaolin.wang@utas.edu.au

* Correspondence: huachen@tjcu.edu.cn (H.C.); gholamreza.kefayati@utas.edu.au (G.K.); Tel.: +86-15602181196

Received: 22 January 2020; Accepted: 24 February 2020; Published: 1 March 2020

Abstract: The condensate on the surface of the minichannel heat exchanger generated during air cooling substantially reduces the heat transfer performance as it works as an evaporator in the air-conditioning system. This has received much attention in scientific communities. In this paper, the effect of operating parameters on the heat transfer performance of a minichannel heat exchanger (MHE) is investigated under an evaporator working condition. An experimental MHE test system is developed for this purpose, and extensive experimental studies are conducted under a wide range of working conditions using the water-cooling method. The inlet air temperature shows a large effect on the overall heat transfer coefficient, while the inlet air relative humidity shows a large effect on the condensate aggregation rate. The airside heat transfer coefficient increases from 66 to 81 W/(m2·K) when the inlet air temperature increases from 30 to 35 °C. While the condensate aggregation rate on the MHE surface increases by up to 1.8 times when the relative humidity increases from 50% to 70%. The optimal air velocity, 2.5 m/s, is identified in terms of the heat transfer rate and airside heat transfer coefficient of the MHE. It is also found that the heat transfer rate and overall heat transfer coefficient increase as the air velocity increases from 1.5 to 2.5 m/s and decreases above 2.5 m/s. Furthermore, a large amount of condensate accumulates on the MHE surface lowering the MHE heat transfer. The inclined installation angle of the MHE in the wind tunnel effectively enhances heat transfer performance on the MHE surface. The experimental results provide useful information for reducing condensate accumulation and enhancing microchannel heat transfer.

Keywords: minichannel heat exchanger; heat transfer; condensate aggregation

1. Introduction

The minichannel heat exchanger (MHE) is used as a novel condenser due to its advantages, such as high efficiency, compact structure, and low material cost [1,2]. It can be widely applied in automotive air conditioning [3,4] and thermoelectrics [5,6]. However, its shutter structure leads to problems such as the poor ability to discharge the condensate water and quick frosting, which limits its application, particularly in commercial refrigeration and air conditioning systems. Recently, MHEs have attracted more and more attention in the context of building air-conditioning and associated heat exchange elements.

The MHE concept was first proposed by Tuckerman and Pease [7] in the 1980s and, subsequently, widely used in large-scale integrated circuits. Swift et al. [8] developed an MHE that was used in common components (such as the photomultiplier tube). Wajs et al. [9] presented a heat exchanger with mini-jet and cylindrical construction. Li Hui et al. [10] utilized an MHE as a condenser

in beverage cabinets. The study demonstrated that the MHE could offer many advantages, such as reduced refrigerant charge, high efficiency, and low cost. Chao Sheng et al. [11] applied a parallel flow heat exchanger in a heat pump system using a water-cooling method. The results indicated that the performance of the water-cooling method was better than that of the air-cooling method. Meanwhile, Kang and Tseng [12] analyzed the effectiveness and pressure drop in a micro-cross flow heat exchanger using water. The results showed that the heat transfer efficiency of a heat exchanger could be improved by appropriately increasing the pressure drop. Lu and Nnanna [13] carried out an experimental study of fluid flow in a microchannel based on a previous study by Senta and Nnanna [14]. The analysis further pointed out that flow uniformity among the channels largely depended on the shape of the manifolds, length and location of inlet and outlets, and the inlet flow rate. The experimental data also indicated that the microchannel structure had a significant impact on the heat transfer rate for all flow rates [15].

Unlike the minichannel condenser, the development of MHEs as evaporators has been relatively slower due to many factors [16–20]. One prominent and obvious problem of minichannel evaporators is the occurrence of condensation when air is cooled in the evaporator surface; the resulting accumulation of condensed water leads to a sharp decrease in the heat transfer efficiency. In this respect, Patil [21] reviewed the heat transfer characteristics, thermal performance, and parametric effects on the heat transfer of MHEs operating under the frosting, defrosting, and dry/wet operating conditions. Furthermore, many studies [22–25] showed that poor drainage of retention water led to thermal performance degradation under the wet, frosting, and defrosting conditions. Kim et al. [26] found that the improvement in drainage performance was due to the reduced surface tension between the fin surface and water droplets. Sun [27] proved that hydrophilic anticorrosive materials can improve condensate removal and thermal performance.

To further eliminate the condensate problem, Shi Junye et al. [28] conducted experimental studies on heat transfer, pressure drop, and condensate removal of parallel-flow evaporators under stable operating conditions. It was evident that the design of the evaporator affects its heat transfer efficiency. Moallem and Hong's [29] experimental results showed that the frosting time and frost growth rate mainly depended on the surface temperature of the local fins. Based on this research, Moallem and Padhmanabhan [30] proposed a method to measure the growth rate of frost mass and thickness at intervals. The experimental data indicated that the frost growth rate at a given dry bulb temperature was mainly affected by the temperature of the fin surface and the relative humidity of air, while water retention and air velocity played a secondary role in the frosting performance. An and Choi [31] investigated the heat and mass transfer performance of corrugated fins with several different shapes and rows of heat exchangers under dry and wet conditions. The simulation results showed that the overall heat transfer rate in the dehumidifying cases was insensitive to the inlet humidity when operating in the fully wet condition. From these researches above, one can conclude that temperature, relative humidity, and air velocity have large effects on the heat transfer efficiency of heat exchangers.

With regard to the performance of HEs under dry and wet coil conditions, Chen et al. [32] compared the thermal performance of evaporative coolers and Kim et al. [33] measured the airside heat transfer and pressure drop using 30 different aluminum heat exchangers with different louver fin geometrical parameters. Li et al. [34] studied the effects of water retention on the air-source heat pump (ASHP) performance. Experimental data showed that the retention of water on the exchanger surface caused an 11% reduction in heating capacity and a 10% drop in efficiency due to continuous frosting and defrosting cycles. Xu [35] compared the wet and frosting performances of three MHEs. The capacities of samples and air pressure drop differences between 3 samples were in the range of 25.6~56.7% and 35~ 63% respectively when the superficial air velocity was 1 m·s-1. This results showed that the droplets that remained in the fin trough was mainly attributed to the heat exchange decay, which obstructed airflow and increased heat-transfer resistance.

The overall thermal performance of MHEs differs according to different operating conditions. For example, condensation and subsequent latent heat release is different due to under partially wet and fully wet operating conditions. Therefore, it is necessary to explore the behavior and performance of systems operating under wet conditions and develop more efficient thermal systems. Saisai et al. [36] analyzed heat transfer characteristics and flow resistance characteristics. The results indicated that the influence of face velocity on heat transfer was significantly greater than that of water flow. Guojun et al. [37] studied the heat transfer and humidity characteristics on the surface of an MHE. The results showed that an increase in the installation angle enhanced removal of the surface condensate water and the installation angle positively influenced the heat transfer coefficient. Further, Lu et al. [38] pointed out that a non-uniform distribution of both the refrigerant and airflow leads to different degrees of performance attenuation of the heat exchanger. Zhang et al. [39] found that the application of an inclined fin layout (downwind/upwind) could improve the fin efficiency. Wei et al. [40] pointed out that under the sublimation condition, the pressure drop on the airside changed negligibly with time, and condensation first appeared on the leeward side. Mohammed et al. [41] found that the air RH, temperatures, and condensation water quantity significantly affected the heat transfer performance. Yin et al.'s [42] experimental results demonstrated that frost thickness increased in a parabolic manner with time and decreased with an increase in air velocity. Furthermore, the maximum heat transfer increased with an increase in air velocity.

From the above research, researchers have put a lot of effort into improving the performance of a minichannel heat exchanger as an evaporator. However, most researchers only focused on one factor and analyzed the influence of this factor on condensate removal and heat transfer performance of an MHE. The practical application is often simultaneously influenced by many factors. In this paper, the effect of influencing factors on the MHE performance was investigated. A certain range of parameters to determine a means of improving condensate removal, enhancing the heat transfer effect, and bettering the performance of an MHE was identified based on the experimental study. The specific inlet parameter values of air velocity and heat exchanger installation angle were quantitatively and experimentally studied to evaluate their influence on the MHE performance. Furthermore, the characteristics of the airside heat transfer, condensed water accumulation, and condensate removal from the MHE surface were predicted under the condensation condition using dynamic dip testing to assess condensate drainage behavior from the air-side surface of an MHE. This method provides highly repeatable data for real-time drainage. The results of the study provide useful information for engineers and researchers in the design and practical application of MHEs as evaporators.

2. Methods

2.1. Experimental Setup

Figure 1 shows a schematic drawing of the MHE test rig, which consists of a wind tunnel, an MHE, condensate collection plate, chilled water supply system and a set of sensors and piping. The MHE is allocated in the wind tunnel, and the environmental state of the heat exchanger is simulated using an environmental test chamber that can provide all the required test conditions. Chilled water is used as the cold source for the MHE. The chilled water flows through the MHE. The chilled water inlet temperature is 5 °C. It cools the heat exchanger tube and removes heat via convective heat transfer from the windward-side air. An air-cooled chiller (model RO-06a) of a Chinese brand (Ri Ou) is used to provide cooling water. The rated cooling capacity is 16.9 kW. A mass flowmeter (LWGY-15) is installed in the straight water supply pipeline to measure the water flow rate. The armored thermocouple is installed on the water supply and return pipelines to measure the water supply and return temperatures. The water supply and return pipes are equipped with gate valves, which can adjust the water flow. The air-cooled chiller supplies the chilled water to the microchannel heat exchanger in the water-side for cooling air. A condensate collection plate is placed at the bottom of the heat exchanger to collect condensate water dripping into the bucket through the drainage pipe.

The bucket is placed on a weighting meter (electronic scale), which records the weight of the condensate water. This weight is used to calculate the discharge rate of the condensate.

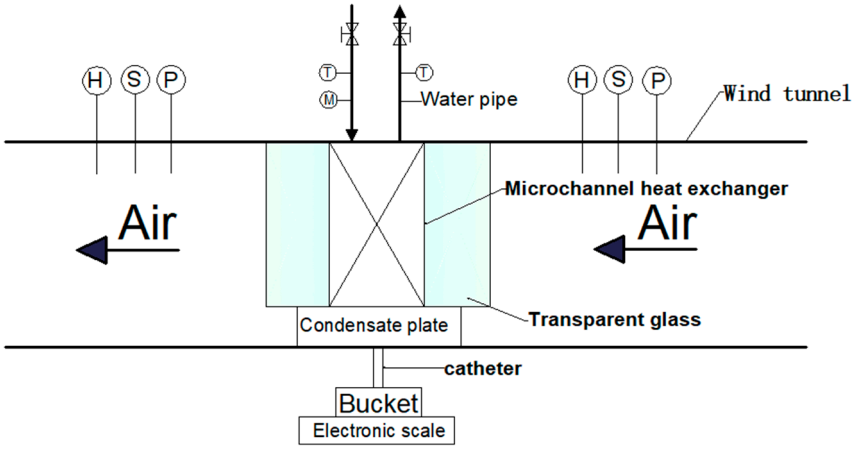

H-Temperature and humidity sensor, P-Differential pressure transducer, S-Multipoint anemometer

T-Armored thermocouple, M -Mass flow meter

Figure 1. Schematic diagram of the minichannel heat exchanger test rig.

The size of the MHE used for our experimental study is 500 × 490 × 32 mm, and the minichannel diameter is 0.8 mm. Figure 2 shows the MHE structural diagram. The heat transfer area is 1.38 m^2 on the chilled water side and 8.33 m^2 on the airside. The inner diameter of the inlet and outlet copper pipes is 14 mm, the outer diameter of the header is 32 mm, and the length of the flat tube is 436 mm. The double-flow form of louver fins is adopted, wherein each flow section contained 24 rows of flat pipes with the header being positioned vertically. The chilled-water inlet and outlet are positioned on the same side of the header, and the connection mode of chilled-water is downward supply and upward return. The water mass flow rate is 1.38 kg/s. The two headers are welded with a movable bracket to allow for adjustment of the inclination of the heat exchanger. The measurement instrument used in the experiments mainly includes temperature and humidity sensors, T-type thermocouples, K-type thermocouples, micro-pressure differential meters, anemometers, liquid-turbine flow meter and electronic weighing meter. Table 1 lists the specifications of the used measurement instruments.

Table 1. Specifications of measurement instruments.

Equipment	Model	Accuracy	Measurement parameter	Measuring range
Thermocouple	K-type	Level 0.5	Water temperature	-40 to 350 °C
Thermocouple	T-type	±0.5 °C	Wall temperature	-200 to 200 °C
Temperature and humidity sensor	AF3020Y	±0.3 °C	Air temperature	-20 to 80 °C
		±2% RH	Relative humidity	0 to 99.9%
Liquid flow meter	LWGY-15	Level 0.5	Water flow	0.6 to 6 m^3/h
Micro-differential pressure gauge	ZP-WB	Level 1	Pressure difference	0 to 1000 Pa
Anemometer	SYSTEM-6242	±0.1 m/s	Air velocity	0 to 20 m/s

In the experiments, the MHE test system is placed in a small room, and air from an outdoor air environment chamber is introduced into the wind tunnel using a variable-frequency fan. The air

velocity is measured using an anemometer (SYSTEM-6242). At the exit of the wind tunnel, the anemometer measures nine points, which are equally allocated on the cross-section of the wind tunnel. Then, the average velocity of the nine measurement points is considered as the studied air velocity. The temperature and humidity sensors are used to monitor the air temperatures and humidity before and after the MHE. The heat transfer capacity, heat transfer coefficient, and condensate removal rate are calculated to analyze the heat transfer characteristics and surface condensate drainage characteristics. The inlet air temperature in the experiment varies from 30 to 35 °C, the air velocity ranges from 1.5 to 3.0 m/s (i.e., air mass flow rate varies from 12.5 to 24.9 kg/s), and the installation angle varies from 0 to 20°.

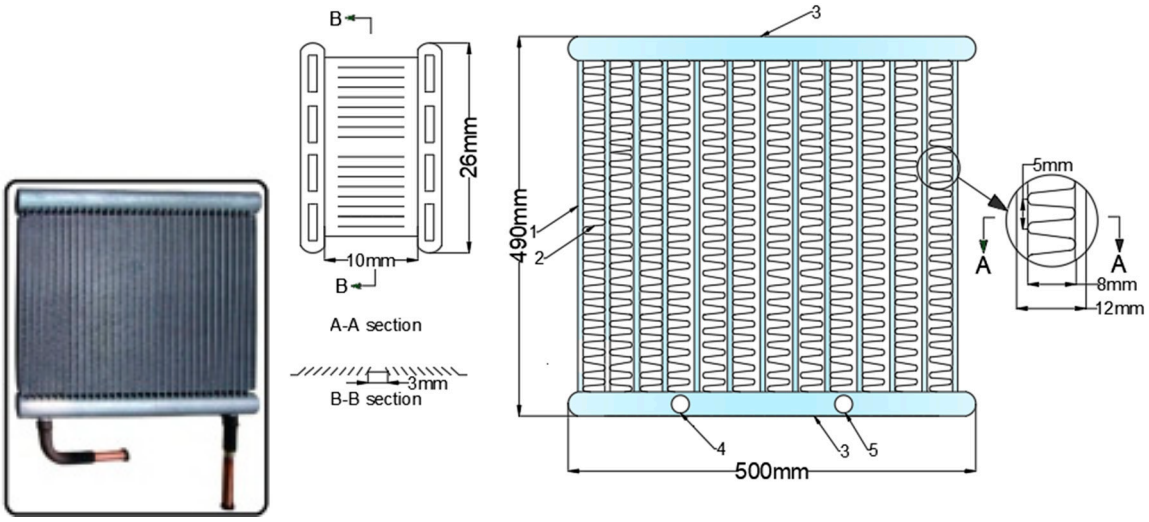

1—flat tube, 2—louver fins, 3—header pipe, 4—refrigerant inlet, 5—refrigerant outlet

Figure 2. Schematic diagram of the minichannel heat exchanger.

2.2. Calculations

The main performance parameters of the MHE are heat transfer, overall heat transfer coefficient, and condensation water removal rate. The heat transfer is calculated based on Equation (1). The air enthalpy is calculated by adapting the NIST(National Institute of Standards and Technology) Refprop [43] simulation tool and verified by a psychrometric chart, as shown in Figure 3. For a given air temperature and RH, the enthalpy and absolute moisture content can be obtained from the NIST Refprop and verified by the psychrometric chart, and can then be used to calculate the heat transfer and condensation water production rate, respectively.

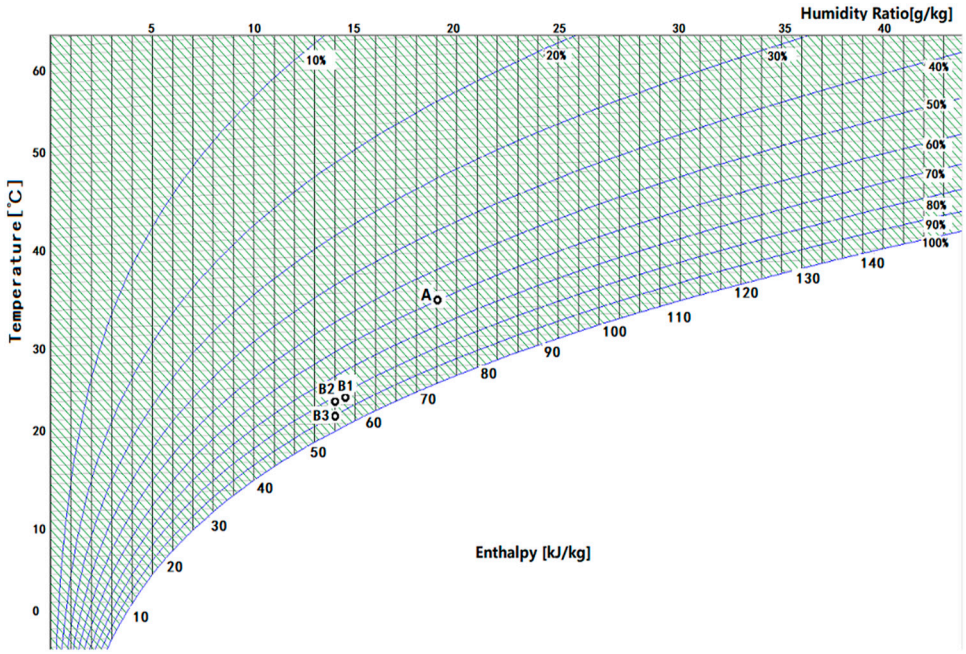

Figure 3. Psychrometric chart.

The heat transfer on the air-side of the MHE is calculated by the following equation:

$$Q_{\mathrm{a}} = \dot{m}_a \left(h_1 - h_2\right) - \dot{m}_w h_{\mathrm{c}} \tag{1}$$

where $\dot{m}_{\mathrm{a}}$ is dry air mass flow rate., kg/s, h_1, and h_2 are air specific enthalpy at inlet and outlet, respectively, kJ/kg. h_c is a specific enthalpy of the condensate. $\dot{m}_w$ is the condensate mass flow rate and is calculated by:

$$\dot{m}_w = \dot{m}_a \cdot \left(w_1 - w_2\right) \tag{2}$$

where, w_1 and w_2 are moisture content of the air at the inlet and outlet of the wind tunnel, kg water/kg of dry air.

$$m = \rho \mathrm{U} A_c \tag{3}$$

$$m = m_a (1 + w_1) \tag{4}$$

where m is *wet* air mass flow rate, kg/s, $\dot{m}_{\mathrm{a}}$ is dry air mass flow rate, kg/s, p is air density, kg/m^3. U is air average velocity, m/s, A_c is the wind cross area, m^2

The heat transfer on the water-side of the MHE is calculated by the following equation:

$$Q_\omega = \mathrm{C}_{\rho\omega} m_\omega \Delta T_\omega \tag{5}$$

where $C_{\rho\omega}$ is the specific heat capacity of water, $\mathrm{m_w}$ is the mass flow rate of water, ΔT_m is the temperature difference between the water inlet and outlet and is calculated by:

$$\Delta T_w = T_{wout} - T_{win} \tag{6}$$

According to the heat balance method, we can know that:

$$Q_a = Q_\omega \tag{7}$$

The overall heat transfer coefficient of the MHE is calculated using the following equation:

$$K = \frac{Q}{A \cdot \Delta T_{\mathrm{m}}} = \frac{Q_a}{A \cdot \Delta T_m} = \frac{Q_w}{A \cdot \Delta T_m} \tag{8}$$

where, K is the overall heat transfer coefficient; A is the air side surface area of the heat transfer, m²; ΔT_m is the logarithmic mean temperature difference of heat transfer in the heat exchanger, °C.

$$\Delta T_m = \Delta T_1 - \Delta T_2 / \ln(\Delta T_1 / \Delta T_2) \tag{9}$$

where ΔT_1 —the temperature difference between the hot fluid inlet and the cold fluid outlet. ΔT_2 — the temperature difference between the hot fluid outlet and the cold fluid inlet. ln—the natural logarithm.

The Reynolds number on the air side is calculated using the following equation:

$$\mathrm{Re} = \rho v \mathrm{L_p} / \mu \tag{10}$$

where p is the density of the air, v is air velocity across minimum wind cross area, m/s, μ is the dynamic viscosity of air, L_p *is* the louver pitch, m.

The condensation removal rate on the MHE surface is calculated by:

$$\dot{m}_{w1} = \frac{\Delta \mathrm{m}}{\Delta t} \tag{11}$$

where Δt is the period selected when calculating the average condensate removal rate at a certain moment, s; Δm is the condensate weight change, kg.

The surface condensate accumulation rate $\dot{m}_{w2}$ on the MHE was calculated using the following equation:

$$\dot{m}_{w2} = \dot{m}_w - \dot{m}_{w1} \tag{12}$$

The experimental measurement error can be calculated based on the sensor accuracy using error propagation. According to the literature [44], the experimental result R is assumed to be calculated from a set of independent variables, which can be represented by:

$$R = (X_1, X_2, X_3, \ldots X_N) \tag{13}$$

The uncertainty of the measurement of a single variable for the experimental results can be given by:

$$\delta R_{\mathrm{xi}} = \frac{\partial R}{\partial X_{\mathrm{i}}} \delta X_{\mathrm{i}} \tag{14}$$

The experimental uncertainty of the final result R can be determined by combining uncertainties of individual terms by a root-sun-square method:

$$\delta R = \left\{ \sum_{i=1}^{N} \left(\frac{\partial R}{\partial X_i} \delta X_i \right)^2 \right\}^{1/2} \quad (15)$$

Based on the accuracies of the measurement devices shown in Table 1, the uncertainty of the heat transfer coefficient and water removal rate can be calculated via Equations (13)-(15). Based on the experimental data, the uncertainties of the air-side heat transfer rate, water-side heat transfer rate, water removal rate, overall heat transfer coefficient, mass flow rate of air, mass flow rate of water, enthalpy of air and moisture content are 4.5%, 3.5%, 4.5%, 5.5%, 2.2%, 0.7%, 3.1% and 2.9%, respectively.

4. Results and discussion

In order to minimize the measurement error in the air-side measurement, the heat balance between the water and air sides of the heat exchanger is calculated and checked. Figure 4 shows the comparison of the heat transfer rate between the water and air sides. The results showed that the discrepancy between the water and air-side heat transfer rate is less than 9.3% over the studied conditions.

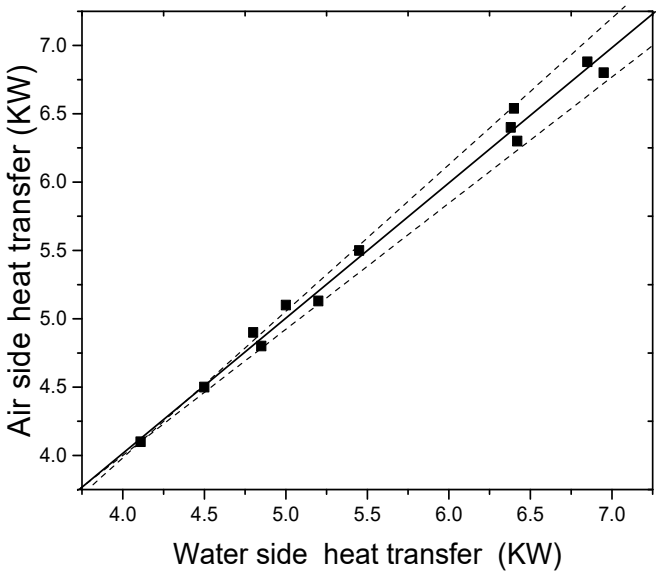

Figure 4. Heat balance comparison chart.

Figure 5 shows the variation of the air outlet temperature under different working conditions. The inlet air temperature varies from 30 to 35 °C and the RH changes from 50% to 70%. It was found that the air outlet temperature decreased rapidly in the first 10 min as the thermal energy was removed by the chilled water. Then the air outlet temperature dropped slowly and reached a stable temperature after 25 minutes. Although the relative humidity and air inlet temperature have a bit of an effect on the time to reach the stable condition, as shown in the figure, the heat transfer process could reach a stable condition after 25 minutes in all studied cases.

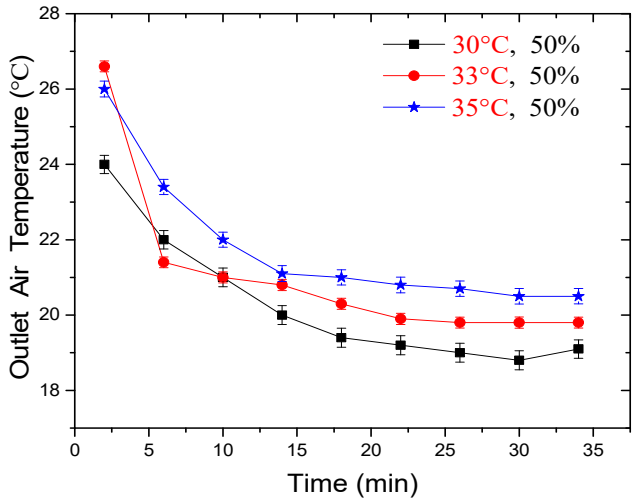

(a) Inlet air temperature from 30 to 35 °C at RH of 50%

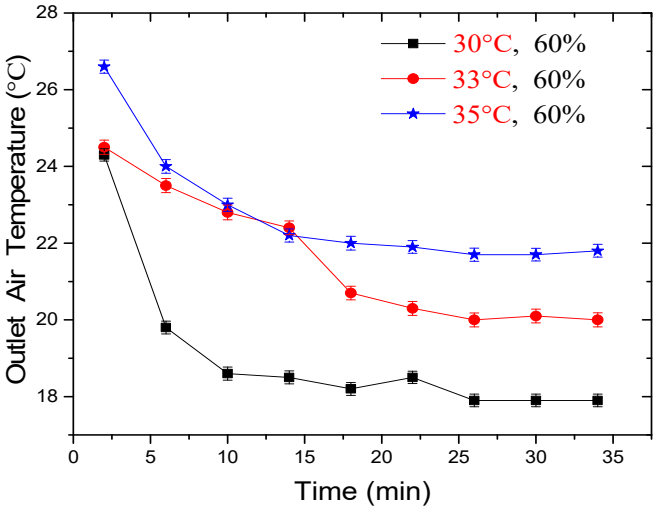

(b) Inlet air temperature from 30 to 35 °C at RH of 60%

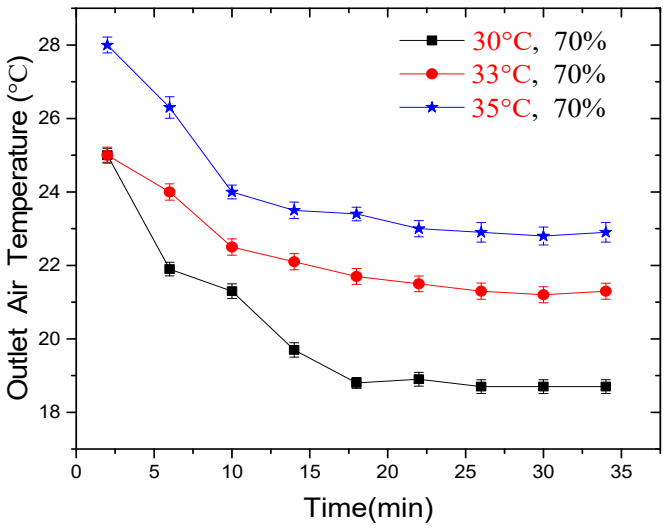

(c) Inlet air temperature from 30 to 35 °C at RH of 60%

Figure 5. Variation of the air temperature at the outlet of the minichannel heat exchanger (MHE) under different air inlet temperatures ($T_{a\text{-}in}$) and relative humidity (RH).

Figure 6a shows the variation of the overall heat transfer coefficient of the MHE under different working conditions. It was found that the overall heat transfer coefficient increased with air inlet temperature. This is caused by the increase of temperature difference between the air inlet and cold water, which substantially enhances the air-side heat exchange in the forced convective heat transfer. Therefore, the overall heat transfer coefficient changes with the air inlet temperature. As the inlet air temperature increased from 30 to 35 °C, the overall heat transfer coefficient increased from 72.5 to 82.5 W/m²·K at an RH of 60%. However, the maximum overall heat transfer coefficient was found at the RH of 60% for each temperature. These changes in the overall heat transfer coefficient could be explained from the air-side heat transfer. As shown in Figure 6b, the air-side heat transfer rate of the MHE increased with the air inlet temperature. However, it was observed that the air-side heat transfer reached the maximum value at RH of 60% for all studied temperatures. This might be due to the fact that the increasing of RH causes the increasing of latent heat exchange and the total heat transfer, but at the same time, the condensate accumulation on the MHE surface, as shown in Figure 7, which results in the decrease of heat transfer. The combined effect results in the optimal heat coefficient occurring at RH of 60%.

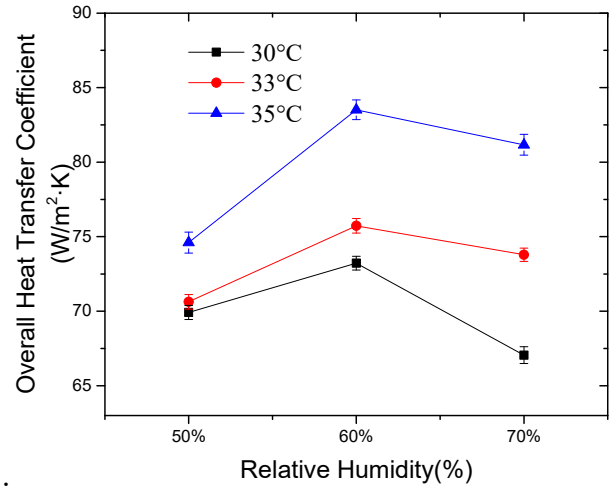

(a)

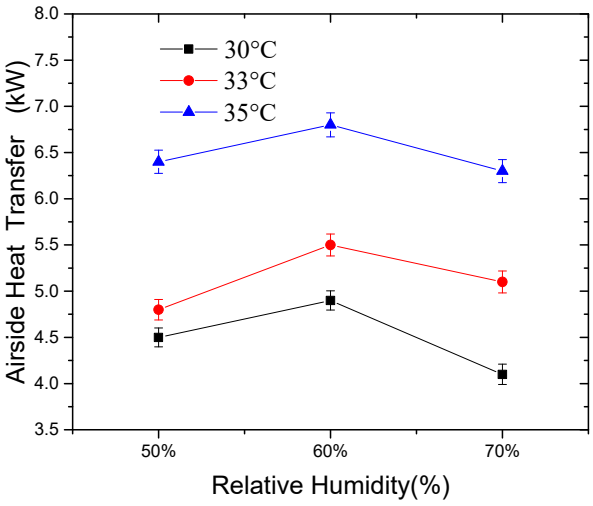

(b)

Figure 6. Variation in the overall heat transfer coefficient and air-side heat transfer under different air inlet temperatures ($T_{a\text{-}in}$) and relative humidity.

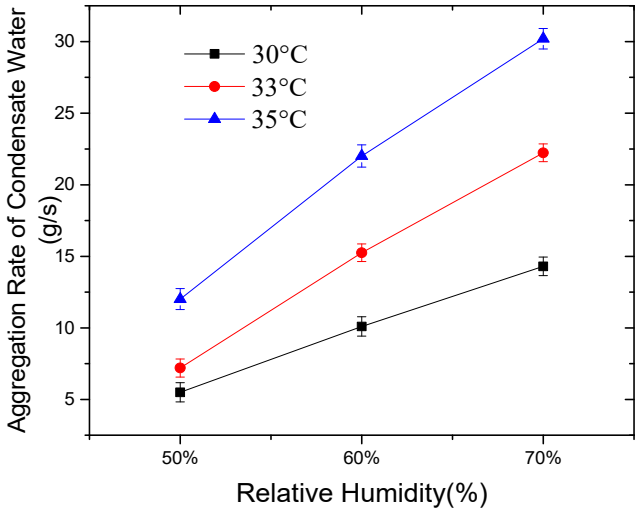

(a)

Figure 7(a). Condensate aggregation rate under different temperatures and relative humidities.

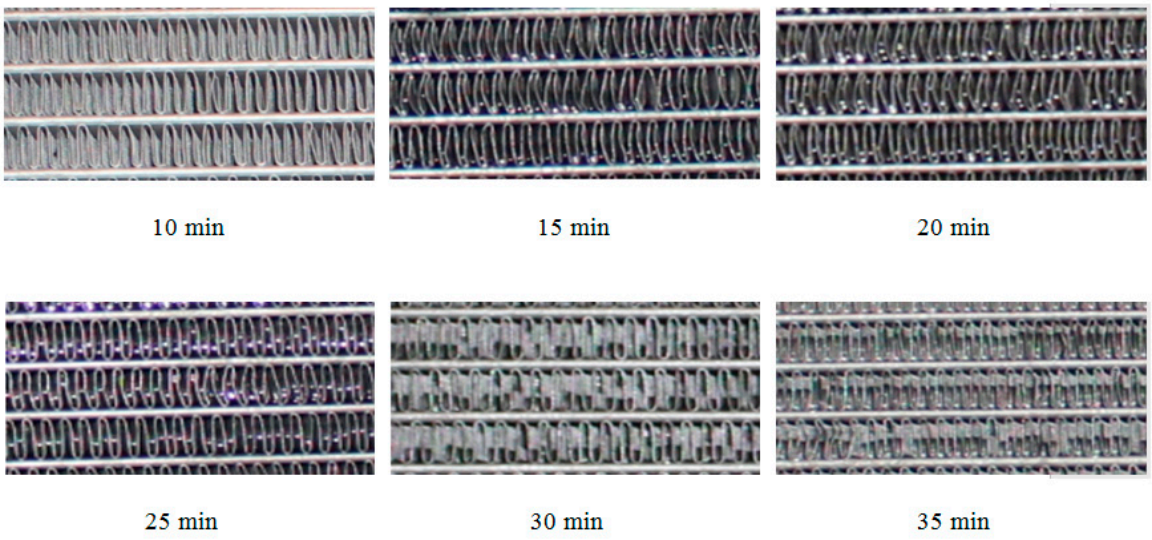

(b)

Figure 7(b). Pictures of the condensate aggregation map at a temperature of 30 °C and relative humidity of 50%.

Figure 7a shows the condensate aggregation rate under different working conditions. As the RH increased from 50% to 70%, the condensate aggregation rate increased by up to 1.8 times. This was because more moisture was contained in the air with high RH at a given temperature. When the air was cooled, more moisture was condensed from the air with high HR. It was also found that the condensate aggregation rate increased with the temperature. This could also be explained by the moisture contained in the air. At the high temperature, more moisture was contained in the air, although the RH is the same. As shown in Figure 7a, the condensate aggregation rate was significant. Under a condition of inlet air temperature of 35 °C and 70% RH, the condensate water accumulation

rate reached 30.2 g/s. This could lead to the rapid blockage of the MHE fins, which might significantly affect the heat transfer rate of the MHE. Figure 7b shows pictures of condensate accumulation on the MHE surface taken by a high definition camera under the working condition of inlet air temperature, 30°C and RH 50%. It was observed that the condensate starts to accumulate after 20 min when the system reached a stable condition. The condensation amount was significant after 30 min. The condensate on the MHE surface could gradually block the airflow, which in turn significantly affected the heat transfer between the air and MHE surface. This explained why the air-side heat transfer reached an optimal value at the RH of 60% and decreased as the RH increased beyond 60%.

Figure 8 shows the variation in the air outlet temperature, MHE air-side heat transfer and overall heat transfer coefficient, and condensate rate under different air velocities. The inlet air temperature and relative humidity were set at 33 °C and 60%, respectively. The air velocity varied from 1.5 to 3.0 m/s in steps of 0.5 m/s. As shown in Figure 8a, both the air outlet temperature and air-side pressure drop increase with increased air velocity. As the air velocity increased from 1.5 m/s to 3.0 m/s, the air outlet temperature increased by 3.7 °C. This rise in the air outlet temperature was mainly because increasing the air velocity increased the air mass flow rate across the MHE and reduced the heat transfer time as the air flowed through the MHE. The air-side pressure drop was found to be increased by 61.1%. This was mainly caused by the high speed of the air.

Figure 8b shows that both the air-side heat transfer and the overall heat transfer coefficient increased initially and dropped after the air velocity was above 2.5 m/s. As the air velocity increased, both air Reynolds number and the amount of air contacting the MHE surface increased, which enhanced the air-side heat transfer. The dependence of the overall heat transfer coefficients on the Reynolds number on the air-side of the MHE is similar to the air velocity (as is shown in Figure 8c) However, an increase in air velocity shortens the heat exchange time, which led to the reduction of the air-side heat transfer. So the air-side heat transfer and overall heat transfer coefficient were affected by these two factors. As the air velocity increased from 1.5 to 2.5 m/s, the first factor played the major role, and hence, both the air-side heat transfer and the overall heat transfer coefficient increased. As the air velocity is above 2.5 m/s, the latter factor played the major role, and hence, the air-side heat transfer and the overall heat transfer coefficient dropped. The optimal air velocity in the studied cases was around 2.5 m/s.

Figure 8d shows the variation of the condensate formation and removal rate. It was found that the condensate formation rate was much higher than the removal rate. This explained the condensate aggregation on the MHE surface, as shown in Figure 7b. This condensate aggregation also increased the pressure drop of the air. It was also found that the highest condensate rate and removal rate appeared at the air velocity, 2.5 m/s. This could be explained from the air-side heat transfer. The results presented in Figure 8 clearly indicated that the air velocity significantly influenced the air-side heat transfer characteristics.

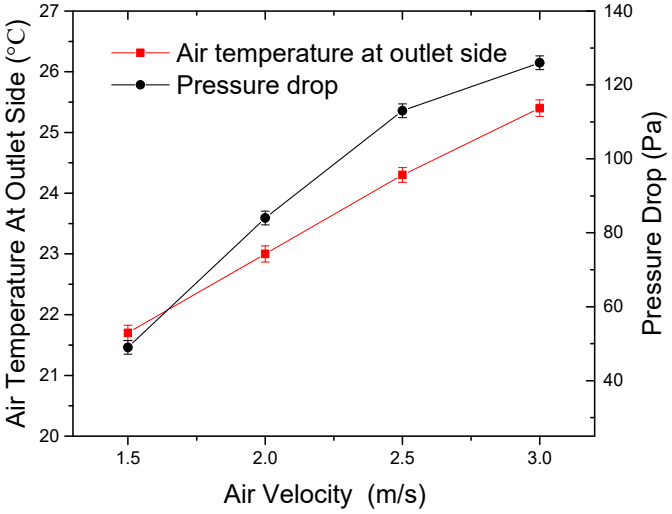
Air temperature at outlet side
Pressure drop
Air Temperature At Outlet Side (°C)
Pressure Drop (Pa)
Air Velocity (m/s)
27
26
25
24
23
22
21
20
140
120
100
80
60
40
1.5
2.0
2.5
3.0

(a)

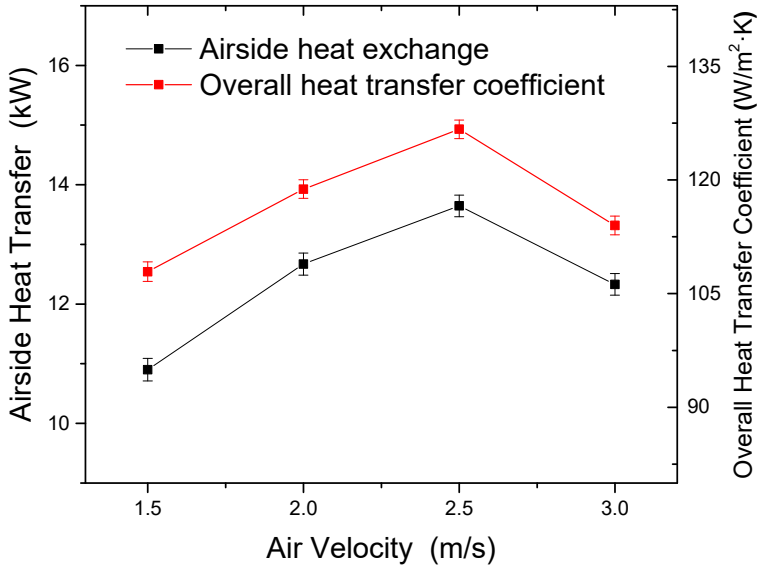
Airside heat exchange
Overall heat transfer coefficient
Airside Heat Transfer (kW)
Overall Heat Transfer Coefficient (W/m²·K)
Air Velocity (m/s)
16
14
12
10
135
120
105
90
1.5
2.0
2.5
3.0

(b)

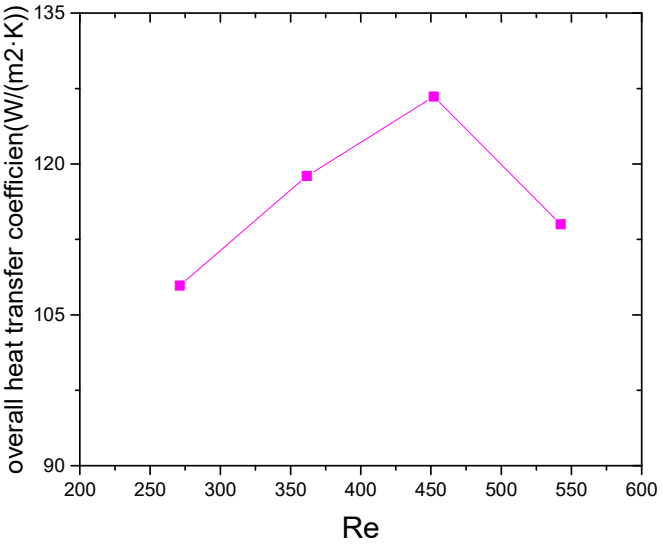

(c)

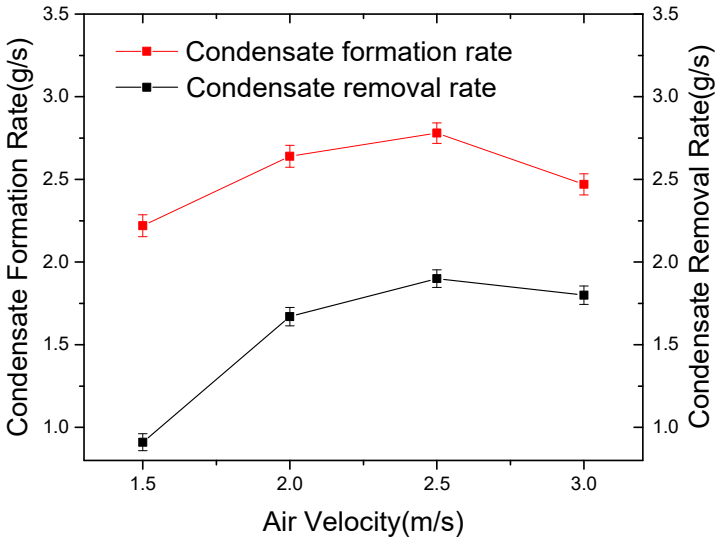

(d)

Figure 8. Variation in heat transfer characteristics under different air velocities: (a) air outlet temperature, (b) the air-side heat transfer and overall heat transfer coefficient, (c) Re and overall heat transfer coefficient and (d) condensate rate.

Figure 9 shows the schematic drawing of the MHE installation in the wind tunnel. The air inlet temperature and relative humidity were maintained at 33 °C and 60%, respectively.

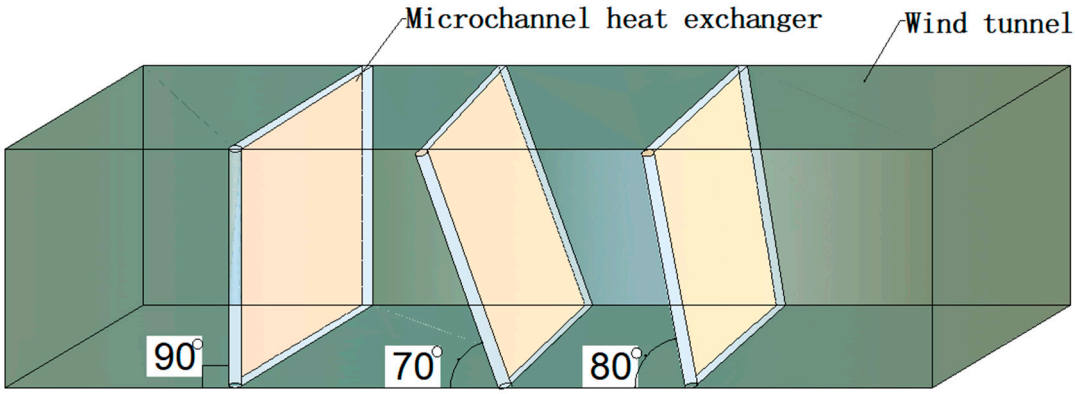

Figure 9. A schematic drawing of the MHE installation in the wind tunnel.

Figure 10a shows the air-side heat transfer and overall heat transfer coefficient under different inclined installation angles in the vertical direction. It was found that the total heat transfer did not change significantly, while the overall heat transfer coefficient increased slightly as the inclined installation angle increased from 0 to 20 °C. This increase in the overall heat transfer coefficient might be due to the condensate aggregation rate. As the inclined angle increased, the condensate aggregation rate decreased as the condensate dropped to the collection plate due to the gravity force. This can be evidenced by the pressure drop, as shown in Figure 10b. In Figure 10b, the air outlet temperature decreased as the inclined installation angle increased. This indicated that the air-side heat transfer increased as the inclined installation angle increased from 0 to 20 °C. As shown in Figure 10c, the condensate water accumulation rate did not change significantly if the measurement error was considered as the inclined installation angle changed from 0° to 10°. However, the condensate accumulation rate reduced substantially from 1.01 to 0.55 g/s as the inclined installation angle changed from 10° to 20°. This was because the inclined installation enhanced the condensate removal rate caused by gravity.

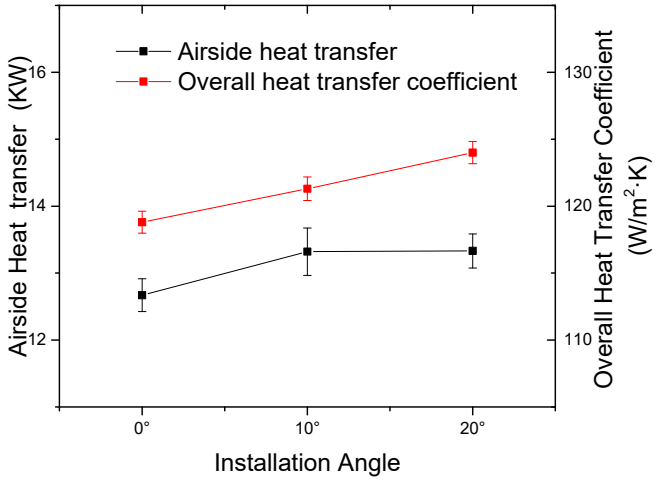

(a)

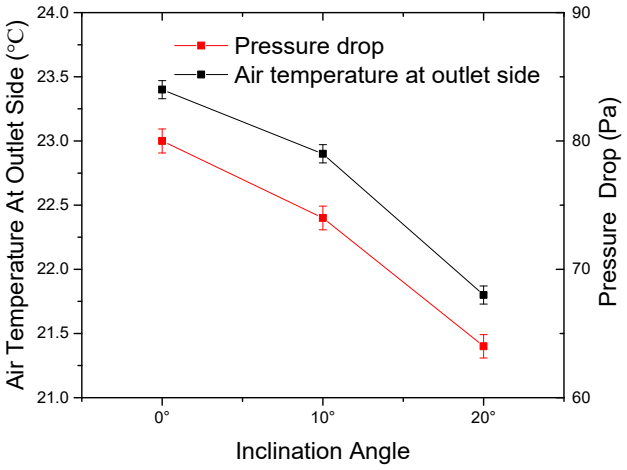

(b)

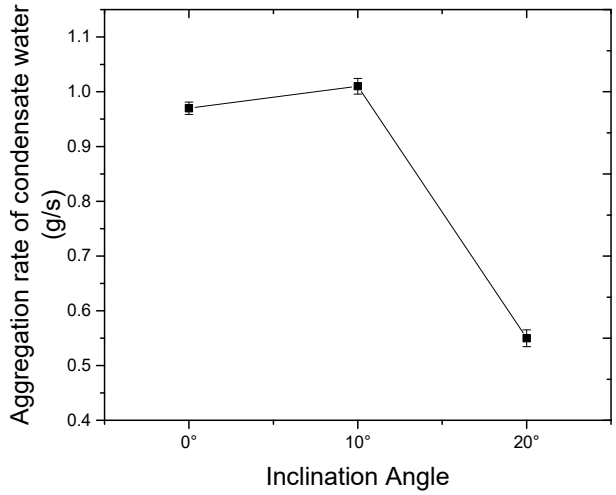

(c)

Figure 10. Variation in heat transfer characteristics under different inclined installation angles to the vertical direction.

5. Conclusions

In this study, an MHE test system was developed to investigate the influence of inlet air temperature, air velocity, and inclined installation angle of MHE on the surface condensate aggregation/removal and heat transfer performance of the MHE used as evaporators. Some specific conclusions were drawn as below:

- Both air inlet temperature and relative humidity showed a large effect on the overall heat transfer coefficient and condensate aggregation rate. As the inlet air temperature increased from 30 to 35 °C, the overall heat transfer coefficient increased from 72.5 to 82.5 W/(m2·K) at 60% RH. An optimal heat transfer coefficient was found at 60% RH for each temperature. The condensate aggregation rate on the MHE surface increased with both air inlet temperature and relative humidity.
- The air velocity also showed a significant effect on the heat transfer characteristics of the MHE. The outlet air temperature and pressure drop across the MHE increased as the air velocity

increased from 1.5 to 3 m/s. However, analysis of air-side heat transfer, overall heat transfer coefficient and condensate aggregation rate showed that 2.5 m/s is the optimal air velocity that achieves the best heat transfer performance. Furthermore, the MHE aggregation rate was much higher than the condensate removal rate, which indicated significant condensate accumulation on the MHE surface under certain conditions.

- The results also showed that the outlet air temperature and pressure drop reduced with the increase in the inclined installation angle. This indicated that the inclined installation of the MHE would enhance the heat transfer performance of the MHE. The heat transfer coefficient increased substantially, and the condensate aggregation rate decreased sharply as the inclined installation angle increased from 10 to 20°.

This experimental study provides useful information for future theoretical studies. It also provides important information for engineers and researchers in the application of MHE as evaporators.

Author Contributions: conceptualization, H.C. and G.K; methodology, X.L and X.W; validation, X.L, H.C and X.W; formal analysis, X.L; investigation, X.L; resources, H.C; data curation, X.L; writing—original draft preparation, X.L and H.C; writing—review and editing, H.C, X.W and G.K; supervision, H.C. All authors have read and agreed to the published version of the manuscript.

Funding: The research was financially supported by the Tianjin Natural Science Foundation of China, grant number: 18JCYBJC90300 and was conducted at the Tianjin Key Laboratory of Refrigeration Technology.

Acknowledgments: The research was financially supported by the Tianjin Natural Science Foundation of China (No.18JCYBJC90300) and was conducted at the Tianjin Key Laboratory of Refrigeration Technology. The first author also acknowledges editing support from the Editage Team in Shanghai.

Conflicts of Interest: The authors declare no conflict of interest. The funders had no role in the design of the study; in the collection, analyses, or interpretation of data; in the writing of the manuscript, or in the decision to publish the results.

References

1. Man-Hoe Kim; Sang Yong Lee; Sunil S; Mehendale,Ralph L. Webb. Microchannel Heat Exchanger Design for Evaporator and Condenser Applications. *Advances in Heat Transfer*,**2003**,*20*,37-42.
2. Qi, Z.G. *Research on Performance Optimization of Automotive Air Conditioning Components and Systems*; Shanghai Jiaotong University: Shanghai, China, 2008.
3. Ding, H.X.; Wang, L.; Ren, N. Microchannel heat exchanger and its application prospect in refrigeration and air conditioning. *Refrig. Air Cond.* **2011**, *11*, 111–115.
4. .Zhao S.T.; Chen H.; Li Y.T.; Experimental study on heat transfer characteristics and its influence of microchannel heat exchanger under *condensation* condition. *Fluid machinery*, **2019**,*47, 60-63*
5. Juliette, S.; Gabin, G.; Bhuvanesh, S. Influence of Ag, Exploring the thermoelectric behavior of spark plasma sintered Fe7-xCoxS8 compounds. *J. Alloy. Compd.* **2020**, *819*, doi:10.1016/j.jallcom.2019.152999.
6. Srinivasan, B.; Gellé, A.; Halet, J.-F.; Boussard-Pledel, C.; Bureau, B. Detrimental Effects of Doping Al and Ba on the Thermoelectric Performance of GeTe. *Materials (Basel Switz.)* **2018**, *11*, .doi:10.3390/ma11112237
7. Tckemran, D.B.; Pease, R.E.W. High-Perfommance heat sikning for VLSI. *IEEE Electron Deviee Lett.* **2020**, *2*, 126–129.
8. Swift, G.; Migliori, A.; Wheatley, J. Microchannel crossflow fluid heat exchanger and method for its fabrication. *J. Heat Recover. Syst.* **1986**, *6*, doi:10.1016/0198-7593(86)90218-3.
9. Wajs, J.; Bajor, M.; Mikielewicz, D. Thermal-Hydraulic Studies on the Shell-and-Tube Heat Exchanger with Minijets. *Energies* **2019,** *12*, 3276, doi:10.3390/en12173276.
10. Li, H.; Yu, Y.; Niu, X.C.; Ma, L.B.; Zhang, Y.H. Experimental study on the application of microchannel heat exchanger in beverage cabinet. *Househ. Appl.* **2014**,*34*, 63–66.
11. Wang, C.S. *Research on the Application of Parallel Flow Heat Exchanger in River Source Heat Pump*; Chongqing University: Chongqing, China, 2009.

12. Kang, S.W.; Tseng, S.C. Analysis of effectiveness and pressure drop in micro crossflow heat exchanger. *Appl. Eng.* **2007**, *27*, 877–85.
13. Lu, X.; Nnanna, A.G.A. Experimental study of fluid flow in microchannel, int. In Proceedings of the ASME 2008 International Mechanical Engineering Congress and Exposition, Boston, MA, USA, 31 October–6 November 2008; pp. 658–679.
14. Senta, M.; Nnanna, A.G.A. Design of manifold for nanofluid flow in microchannels. In Proceedings of the ASME International Mechanical Engineering Congress and Exposition, Seattle, DC, USA, 11–15 November 2007; pp. 1–8.
15. Mohammed, H.A.; Bhaskaran, G.; Shuaib, N.; Saidur, R. Heat transfer and fluid flow characteristics in microchannels heat exchanger using nanofluids: A review. *Renew. Sustain. Energy Rev.* **2011**, *15*, 1502–1512.
16. Liu, S.; Hu, Y.X.; Huang, X.Z. Application analysis of microchannel heat exchanger in the compression and condensation unit. *Refrig. Air Cond.* **2010**, *24*, 31–34.
17. Yin, X.W.; Wang, W.; Patnaik, V.; Zhou, J.S.; Huang, X.C. Evaluationof microchannel condenser characteristics by numerical simulation. *Int. J. Refrig.* **2015**, *54*, 126–141.
18. Shao, L.L.; Yang, L.; Zhang, C.L. Comparison of heat pump performance using fin-and-tube and microchannel heat exchangers under frost conditions. *Appl. Energy* **2010**, *87*, 1187–1197.
19. Zhang, X.; Jia, L.; Qi, P.; Chao, D. Comparison of heat pump performance using fin-and-tube and microchannel heat exchangers under frost conditions. *Appl. Therm. Eng.* **2019,** *152*, 196–203.
20. Siddiqui, O.K.; Zubair, S.M. Efficient energy utilization through proper design of microchannel heat exchanger manifolds: A comprehensive review. *Renew. Sustain. Energy Rev.* **2017**, *74*, 969–1002.
21. Patil, M.S.; Seo, J.H.; Lee, M.Y. Heat transfer characteristics of the heat exchangers for refrigeration, air conditioning and heat pump systems under frosting, defrosting and dry/wet conditions—A review. *Appl. Therm. Eng.* **2017**, *113*, 1071–1087.
22. Kim, K.M.; Kim, M.H.; Kim, D.R.; Lee, K.S. Thermal performance of microchannel heat exchangers according to the design parameters under the frosting condition. *Int. J. Heat Mass Trans.* **2014**, *71*, 626–632.
23. LAN S.W.;Pei Y.;Ding G.L. Refrigerant distribution characteristics of microchannel evaporator under frosting condition. Journal of refrigeration, **2019**,*40*: 43-49..
24. Gong, J.; Gao, T.; Yuan, X.; Huang, D. Effects of air flow maldistribution on refrigeration system dynamics of air source heat pump chiller under frosting conditions. *Energy Convers. Manag.* **2008**, *49*, 1645–1651.
25. Liu, Z.; Li, X.; Wang, H.; Peng, W. Performance comparison of air source heat pump with R407C and R22 under frosting and defrosting. *Energy Convers. Manag.* **2008**, *49*, 232–239.
26. Kim, M.H.; Kim, H.; Kim, D.R.; Lee, K.S. A novel louvered fin design to enhance thermal and drainage performances during periodic frosting/defrosting conditions. *Energy Convers. Manag.* **2016**, *110*, 494–500.
27. Sun, S.P.; Shi, Y.; Liao, Q.; Liu S.T.. Study on the condensate removal of parallel flow evaporator. *Refrig. Air Cond.* **2008**, *8*, 97–100.
28. Shi, J.Y.; Qu, X.; Qi, Z.; Wang Z.K. Study on wet working condition performance of parallel flow evaporator for new automotive air conditioning. *Automot. Eng.* **2011,** *33*, 74–78.
29. Moallem, E.; Hong, T.; Cremaschi, L.; Daniel, E.F. Experimental investigation of adverse effectof frost formation on microchannel evaporators, part1: Effect of fin geometry and environmental effects. *Int. J. Refrig.* **2013**, *36*, 1762—1775.
30. Moallem, E.; Padhmanabhan, S.; Cremaschi, L.; Fisher, D.E. Experimental investigation of the surface temperature and water retention effects on the frosting performance of a compact microchannel heat exchanger for heat pump systems. *Int. J. Refrig.* **2012**, *35*, 171—186.
31. An, C.S.; Choi, D.H. Analysis of heat transfer performance of cross-flow fin-tube heat exchangers under dry and wet conditions. *Int. J. Heat Mass Trans.* **2012**, *55*, 1496–1504.
32. Feng, Y.C. Mal-defrost accident research of air source heat pump. Master's Thesis, Beijing University of Technology, Beijing, China, 2013.
33. Kim, M.H.; Bullard, C.W. Air-side performance of brazed aluminum heat exchangers under dehumidifying conditions. *Int. J. Refrig.* **2002**, *25*, 924–934.
34. Li, L.T.; Wang, W.; Sun, Y.Y.; Feng, Y.C.; Lu, W.P.; Zhu, J.H.; Ge, Y.J. Investigation of defrosting water retention on the surface of evaporator impacting the performance of air source heat pump during periodic frosting–defrosting cycles. *Appl. Energy* **2014**, *135*, 98–107.

35. Xu, B.; Zhang, C.; Wang, Y.; Chen, J.P.; Xu, K.H.; Li, F.; Wang, N.J. Experimental investigation of the performance of microchannel heat exchangers with a new type of fin under wet and frosting conditions. *Appl. Therm. Eng.* **2015,** *89*, 444–458.
36. Han, S.S.; liu, J.H.; Zhao, Y.J.; Zhang, L. Research on the heat transfer performance of parallelflow heat exchangers for automotive air conditioning and heating systems. *Enery Res. Inf.* **2016,** *32*, 207–211.
37. He, G.J. Research progress on reliability of microchannel heat exchanger for air conditioning. *Refrigeration* **2014,** *2*, 45–48.
38. Lu, H.L.; Tao, H.G.; Hu, Y.P.; Hu, H.M.; Jin, K.X.; Chen, H.X. Research progress on the uniformity of thermal fluid distribution in parallel flow heat exchangers. *Acta Refrig. Sin.* **2010,** *31*, 39–45.
39. Zhang, H.Y.; Li, J.M.; Wang, B.X. Application of microchannel heat exchanger in household air conditioning. *HVAC* **2009,** *39*, 80–85.
40. Sheng, W.; Liu, P.P.; Ding, G.L. Experimental study on frosting performance of microchannel heat exchanger. *Fluid Mach.* **2017,** *45*, 60–65.
41. Mohammed, H.A.; Bhaskaran, G.; Shuaib, N.H.; Abu-Mulaweh, H.I. Influence of nanofluids on parallel flow square microchannel heat exchanger performance. *Int. Commun. Heat Mass Transf.* **2010**, *38*, 1–9.
42. Yin, C.X.; Chen, Y.G. Effect of wind speed on frosting characteristics of finned tubeheat exchanger of air source heat pump. *Low Temp. Supercond.* **2011,** *39*, 50–52.
43. Available online: https://webbook. nist. gov/chemistry/ (accessed on 2020.1.19).
44. Holman, J.P. *Experiment Method for Engineers*, 6th ed.; McGraw-Hill: Singapore, 1994.